



# Nonlinear characterization of silica and chalcogenide microresonators

JIANGANG ZHU,<sup>1,\*</sup> MO ZOHRABI,<sup>1</sup> KYUYOUNG BAE,<sup>1</sup> THOMAS M. HORNING,<sup>2</sup> MICHAEL B. GRAYSON,<sup>1</sup> WOUNJHANG PARK,<sup>1</sup> AND JULIET T. GOPINATH<sup>1,2</sup> 

<sup>1</sup>Department of Electrical, Computer and Energy Engineering, University of Colorado Boulder, 425 UCB, Boulder, Colorado 80309, USA

<sup>2</sup>Department of Physics, University of Colorado Boulder, 425 UCB, Boulder, Colorado 80309, USA

\*Corresponding author: [jiangang.zhu@colorado.edu](mailto:jiangang.zhu@colorado.edu)

Received 26 February 2019; revised 24 April 2019; accepted 1 May 2019 (Doc. ID 361074); published 23 May 2019

Microresonators offer an attractive combination of high quality factors and small optical mode volume. They have emerged as a unique platform for the study of fundamental physics and for applications ranging from exquisite sensors to miniature optical combs. Characterizing the linear and nonlinear properties of a microresonator is the first step toward new applications. Here, we present a novel *in situ* method to measure the nonlinear refractive index and absorption coefficient in microresonators. Laser-scanned transmission spectra are fitted by a comprehensive theoretical model that includes the thermo-optic effect, Kerr effect, and back-coupling of counter-propagating modes. The effectiveness of our technique is demonstrated by evaluating the nonlinear indices and optical absorption of silica and chalcogenide ( $\text{As}_2\text{S}_3$ ) microspheres at 1.55  $\mu\text{m}$ . Significantly, our method also quantifies important parameters including the quality factor, thermal relaxation time, and back-coupling coefficient at the same time. Our findings provide a powerful new approach for characterization of microresonators and optical materials and pave the way for new opportunities in the area. ©2019

Optical Society of America under the terms of the [OSA Open Access Publishing Agreement](#)

<https://doi.org/10.1364/OPTICA.6.000716>

## 1. INTRODUCTION

Nonlinear optical materials are crucial for novel light sources [1], optical memories [2], and communications components [3]. The precise measurement of Kerr nonlinearity (the nonlinear refractive index  $n_2$ ) is essential to the analysis, design, and use of nonlinear devices. In bulk optical materials, the  $z$ -scan technique is often used for measuring nonlinearity. The sample material is moved through the focus of a strong laser beam, which induces self-focusing [4]. However, the technique is not suitable for thin films and is challenging to implement. In thin films and waveguides, spectral broadening occurs as a result of self-phase modulation when a laser pulse is transmitted through the nonlinear material, and  $n_2$  can be estimated by analyzing the broadened spectrum [5]. This method is effective, but the technique works only for certain device configurations.

Furthermore, microresonators have emerged as a unique platform for studying fundamental physics and as an integrated photonic component. Different types of resonator geometries such as microspheres, toroids, bottles, rods, capillaries, and integrated micro-rings and disks [6] have found applications in lasing [7,8], biological and chemical sensing [9,10], optical communications [3], optomechanics [11], frequency combs [12], and non-Hermitian physics [13]. The very high quality factors ( $Q$ ) and small mode volumes of these devices result in strong light-matter interaction and enable nonlinear phenomena including the self-/cross-phase modulation, harmonic generation, four-wave mixing [14], and Raman [7] and Brillouin scattering [15]. To design and characterize these devices, a rigorous

understanding of the underlying nonlinear physics is essential. Therefore, a convenient and *in situ* way to measure  $n_2$  and other parameters in microresonators is critical.

Scanning a single frequency probe laser across resonance is a common way to obtain the resonance lineshape in microresonators. Various nonlinear phenomena have been observed in the transmission spectra by laser scanning, including lineshape broadening and narrowing, pulsing, ringing, and oscillation [14,16–19]. Information on the magnitude of the nonlinearity and linear absorption is manifested in the spectra.

Here, we present an accurate and *in situ* method to measure the nonlinear refractive index ( $n_2$ ) and optical absorption coefficient ( $\alpha$ ) in microresonators. It is based on modeling of the linear and nonlinear effects inside a microresonator during probe laser wavelength scans and fitting the simulated transmission to the experimental spectra. Compared to existing methods, the technique presented here yields far more flexibility and information. It is simple enough to allow *in situ* measurement of microresonators from laser resonance scans, and perfectly suited to characterize microresonators fabricated from thin-film materials or engineered materials, whose optical properties are often different from bulk. Theoretical modeling and experimental measurements of  $n_2$  and  $\alpha$  for silica and  $\text{As}_2\text{S}_3$  microspheres are presented.

## 2. THEORY

In a microresonator, the transmission spectrum of a resonance mode manifests itself as an inverted Lorentzian shape [6].

These resonances are usually observed at a low input power ( $< 10$  nW), where nonlinear effects are difficult to trigger. As the input power increases, the non-negligible amount of material absorption causes heating of the microresonator, and as a result, the resonance wavelength is shifted due to thermal expansion and the thermo-optic refractive index change of the material [16]. This effect manifests itself in the scanned spectra as lineshape broadening and narrowing, depending on the direction of scanning wavelength [16]. Self- and cross-phase modulation (due to Kerr nonlinearity) can also produce lineshape distortion similar to that caused by heating. However, there are differences between these two co-existing phenomena. The Kerr effect is almost instantaneous [20,21], while the thermal effect is slow (characteristic time constant  $> 1$   $\mu$ s) [16,22]. This difference has been exploited to separate the thermal and Kerr effects in measurement, but requires a time-resolved pump-probe setup and amplitude modulation of the pump [20,21]. During lineshape broadening, the overall on-resonance time of the interaction between laser and cavity is prolonged, while during lineshape narrowing, the time length is shortened. The faster dynamics during lineshape narrowing relies more on the fast process (Kerr), while the slower dynamics during lineshape broadening manifest more of the slow process (thermal). Thus, in principle, the narrowed lineshape can be used to better evaluate  $n_2$ , and the broadened lineshape can be used to better evaluate  $\alpha$ .

Figure 1 shows a schematic of a microresonator, optically coupled with a tapered fiber [23]. We consider a theoretical model based on coupled-mode theory, given by the following equations [24]:

$$\frac{dA_{cw}}{dt} = (-\gamma_{\text{tot}} - (\Delta\omega_{cw} - g))A_{cw} - igA_{ccw} - i\frac{\eta}{\tau_0}B_{cw}^{\text{in}}, \quad (1a)$$

$$\frac{dA_{ccw}}{dt} = (-\gamma_{\text{tot}} - (\Delta\omega_{ccw} - g))A_{ccw} - igA_{cw} - i\frac{\eta}{\tau_0}B_{ccw}^{\text{in}}, \quad (1b)$$

$$\frac{dT}{dt} = -\frac{G}{H}(T - T_0) + \frac{\alpha c \tau_0}{H}(|A_{cw}|^2 + |A_{ccw}|^2), \quad (2)$$

$$\Delta\omega_{cw} = \omega_p - \omega_0 \left( 1 - \frac{n_2}{n_0 A_{\text{eff}}} (|A_{cw}|^2 + 2|A_{ccw}|^2) - \frac{dn}{dT} \frac{T}{n_0} \right), \quad (3a)$$

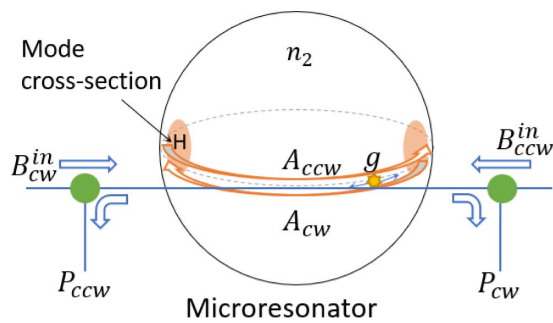


**Fig. 1.** Schematic of the microresonator coupled to a waveguide. Two counter-propagating modes,  $A_{cw}$  and  $A_{ccw}$ , are excited by a waveguide coupler.  $A_{cw}$  and  $A_{ccw}$  are coupled through scatterers with coupling rate of  $g$ . The material of the microresonator has nonlinear index of  $n_2$ , and the thermo-optic mode volume related to direct optical heating is designated as  $H$ . Two circulators are used to separate the counter-propagating modes coupled back to the waveguide.

$$\Delta\omega_{ccw} = \omega_p - \omega_0 \left( 1 - \frac{n_2}{n_0 A_{\text{eff}}} (|A_{ccw}|^2 + 2|A_{cw}|^2) - \frac{dn}{dT} \frac{T}{n_0} \right), \quad (3b)$$

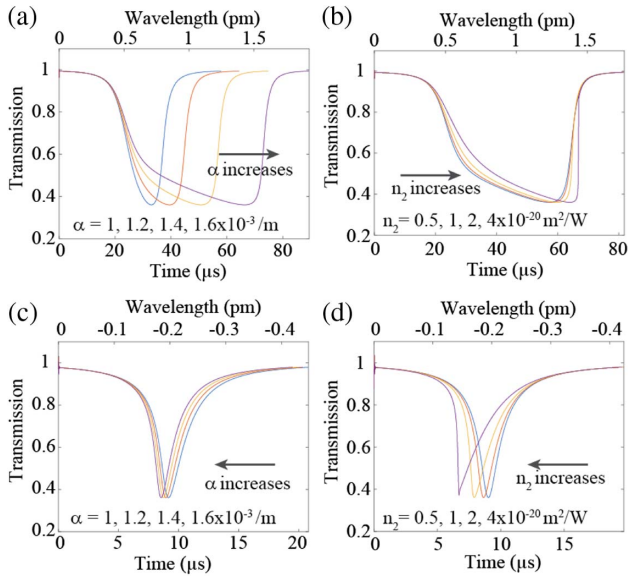
$$P_{cw} = B_{cw}^{\text{in}} - i\eta A_{cw}, \quad (4a)$$

$$P_{ccw} = B_{ccw}^{\text{in}} - i\eta A_{ccw}, \quad (4b)$$

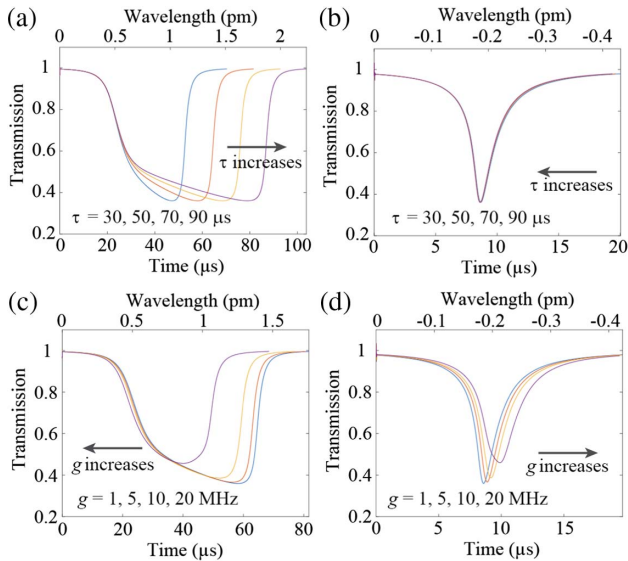
where  $A_{cw}$  and  $A_{ccw}$  represent clockwise (CW) and counter-clockwise (CCW) mode amplitude;  $B_{cw}^{\text{in}}$  and  $B_{ccw}^{\text{in}}$  are input light amplitude into the CW and CCW modes, respectively;  $T$  is temperature of the resonance mode volume;  $\gamma_0$  is the intrinsic loss rate of the resonator,  $\gamma_{\text{ex}}$  is the coupling loss rate, and  $\gamma_{\text{tot}} = \gamma_0 + \gamma_{\text{ex}}$ ;  $g$  is the coupling rate of counter-propagating circulating modes;  $n_2$  is the nonlinear index of the microresonator, and  $n_0$  is the linear refractive index of the resonator;  $A_{\text{eff}}$  is the effective resonance mode area;  $\tau_0$  is the round-trip time of light in the resonator;  $\eta = (2\tau_0\gamma_{\text{ex}})^{1/2}$  is the fiber taper coupling constant; and  $G$  and  $H$  are the thermal conductance and thermal capacity, respectively, of the resonator. Equations (1a) and (1b) are the rate equations of the counter-propagating modes (CW and CCW), where  $\Delta\omega$  is the angular frequency detuning between resonance mode and the probe laser. Scattering in the microresonator can be caused by surface roughness, contamination, and material impurities, and it is almost impossible to avoid it. Therefore, we include back-coupling of CW and CCW modes in the model. The coupling strength of the counter-propagating modes is given by  $g$  in Eqs. (1a) and (1b). Equation (2) describes the thermo-optic heating and thermal transfer inside the microresonator.  $|A_{cw}|^2 + |A_{ccw}|^2$  is the optical power responsible for thermal heating, and  $H$  is the mode volume that experiences direct optical heating by the resonance mode. Environmental temperature is given as  $T_0$ . Equations (3a) and (3b) describe the resonance frequency shift caused by self-phase modulation and cross-phase modulation ( $n_2(|A_{cw}|^2 + 2|A_{ccw}|^2)/n_0 A_{\text{eff}}$ ), as well as temperature increase ( $T dn/n_0 dT$ ). Equations (4a) and (4b) are the waveguide coupling equations for output power in fiber  $P_{cw}$  and  $P_{ccw}$ . To evaluate the system with a linearly wavelength-scanned pump laser, the equations are numerically integrated using Runge-Kutta method to simulate the experimental lineshape. The time step used for the integration is between 1 ns and 4 ns.

Figure 2 illustrates the calculated effects of different  $\alpha$  and  $n_2$  during wavelength upscan and downscan for a silica microsphere. As seen in Fig. 2(a), increasing  $\alpha$  has the effect of increasing thermal heating, and as a result, the lineshape broadening significantly increases with larger  $\alpha$  values during an upscan. On the other hand, in Fig. 2(c), lineshape narrowing is more significant with increasing  $\alpha$  during a downscan. The effect of  $n_2$  is more subtle. In general, increasing values of  $n_2$  causes the lineshape to “tilt” as opposed to broadening or narrowing. As seen in Figs. 2(b) and 2(d), larger values of  $n_2$  increase the skewness of the lineshape. This effect manifests itself better in the narrowed spectra [Fig. 2(d)], as thermal effect is less significant in the narrowed spectra.

Figure 3 illustrates the effects of different thermal constants (defined as  $\tau = H/G$ ). In the broadened spectra, increasing  $\tau$  has the effect of increasing thermal insulation, which enhances thermal heating of the resonance mode volume and further broadens the lineshape [see Figs. 3(a) and 3(b)]. Since increasing  $\alpha$  and  $\tau$  both broaden the spectra significantly during wavelength upscan [see Figs. 2(a) and 3(a)], it is difficult to directly differentiate the



**Fig. 2.** Calculated transmission spectrum of a theoretical microresonator for (a) different  $\alpha$  during wavelength upscan, (b) for different  $n_2$  during wavelength upscan, (c) for different  $\alpha$  during wavelength downscan, and (d) for different  $n_2$  during wavelength downscan. Parameters for calculation: input power: 5 mW; resonator radius: 50  $\mu\text{m}$ ; effective mode area: 15  $\mu\text{m}^2$ ; intrinsic  $Q$  factor:  $2 \times 10^7$ ;  $n_2: 1 \times 10^{-20} \text{ m}^2/\text{W}$ ;  $\alpha: 0.0015/\text{m}$ ; specific heat: 700 J/(kgK); density: 2400  $\text{kg}/\text{m}^3$ .



**Fig. 3.** Calculated transmission spectrum of a theoretical microresonator: (a) during wavelength upscan for different thermal time constant  $\tau = H/G$ , (b) during wavelength downscan for different  $\tau$ , (c) during wavelength upscan for different  $g$ , and (d) during wavelength downscan for different  $g$ . Parameters for calculation: input power: 5 mW; resonator radius: 50  $\mu\text{m}$ ; effective mode area: 15  $\mu\text{m}^2$ ; intrinsic  $Q$  factor:  $2 \times 10^7$ ;  $n_2: 1 \times 10^{-20} \text{ m}^2/\text{W}$ ;  $\alpha: 0.0015/\text{m}$ ; specific heat: 700 J/(kgK); density: 2400  $\text{kg}/\text{m}^3$ .

origination of the broadening (thermal heating or insulation). In the narrowed spectra [Fig. 3(b)], increasing  $\tau$  has little effect compared to the case of broadened spectra. This is because the shorter time duration of the narrowed spectra does not allow significant

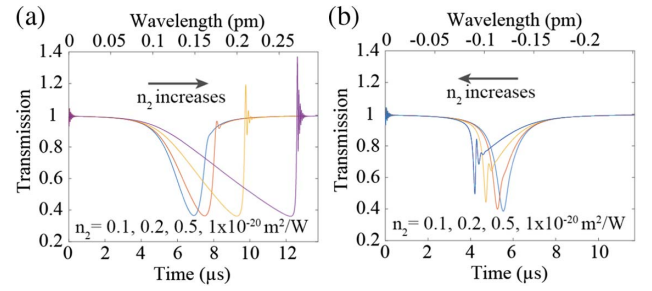


**Fig. 4.** Calculated transmission spectra of a theoretical microresonator showing ringing effect during (a) wavelength upscan and (b) during wavelength downscan. The oscillations at the beginning of the spectra are due to noise in the numerical integration (sensitivity to initial values). Parameters for calculation: input power: 5 mW; resonator radius: 50  $\mu\text{m}$ ; effective mode area: 15  $\mu\text{m}^2$ ; intrinsic  $Q$  factor:  $8 \times 10^7$ ;  $\alpha: 10^{-4}/\text{m}$ ; specific heat: 700 J/(kgK); density: 2400  $\text{kg}/\text{m}^3$ .

thermal buildup. Therefore, the narrowed spectra are more suitable for separating the effect of  $\alpha$  from the effect of thermal time constant.

Figs 3(c) and 3(d) show the effects of different coupling rates ( $g$ ) of counter-propagating modes. As seen in Figs. 3(c) and 3(d), when  $g$  is smaller ( $< 10$  MHz), the effect of increasing  $g$  is similar to reducing coupling strength ( $\eta$ ), where on-resonance transmission is increased (resonance curve moves towards under-coupled-like conditions). Thus, it is hard to separate the effect of  $g$  from the effect of coupling change in lineshape distortions. In the case of larger  $g$  ( $g > \gamma_0 + \gamma_{ex}$ ), mode splitting can be observed, and it has a significant effect on the lineshape. For simplicity and effectiveness of measuring  $n_2$  and  $\alpha$  in experiments, we choose microresonators without a significant amount of mode splitting to simplify discussion.

When the  $Q$  of the microresonator is higher ( $> 10^7$ ), and the input power is increased, a ringing effect is often observed when the scanning laser wavelength crosses the resonance [Figs. 4(a) and 4(b)]. The ringing phenomenon is a fast process and is dominated mostly by the Kerr effect. Oscillations at the beginning of the spectra in Figs. 4(a) and 4(b) are due to noise in the numerical integration (sensitivity to initial values). Previous work has shown that the ringing spectra can be used to extract  $n_2$  [19]. However, this method is not suitable for microresonators with lower  $Q$  factors ( $Q < 10^5$ ), when ringing is hard to achieve. Therefore, in the following experiments and discussion, we will focus on the more general cases where ringing is not visible.

### 3. EXPERIMENTS

We have verified our method experimentally by extracting  $n_2$  and  $\alpha$  from silica and chalcogenide microresonators. To evaluate the theoretical model and study the effects of  $\alpha$  and  $n_2$ , we developed a LabVIEW program using our theoretical model for calculation of spectrum lineshape and manual tuning of the parameters. It is used to roughly fit the experimental data by manually adjusting each parameter, which helps determine the starting ranges of parameters for the genetic algorithm. For experiments, we prepared fresh silica and chalcogenide microspheres by melting the end of silica and  $\text{As}_2\text{S}_3$  tapered fibers, respectively [25]. The resulting silica microsphere has a  $Q$  factor above  $10^7$  and the chalcogenide microsphere, a  $Q$  factor above  $10^6$ . The prepared

microspheres also lack significant mode splitting or back-scattering ( $g$ ), which simplifies our analysis. A silica tapered fiber is fabricated by a heat-and-pull method [23] and is aligned with the microresonators using a 3D stage. A single-frequency mode-hop-free tunable laser in 1550 nm band (Toptica DLC CTL 1550) is used to probe the resonance modes. The laser wavelength is scanned by piezo-actuating the laser cavity with a triangle waveform. An InGaAs photodetector (Newport 1811-FC) is used to measure the transmitted light, and an oscilloscope is used to record data.

### A. Silica Microsphere

We obtained the transmission spectra of a silica microsphere for both wavelength upscan and downscan at five different taper-resonator coupling conditions [Supplement 1, Fig. S1]. These scans were taken in the under-coupled regime, where the loaded  $Q$  factor is higher than in the over-coupled regime. For each coupling condition and scan direction, we captured 10 spectra (100 total). To fit an experimental spectrum, there are six free parameters to adjust, which are  $Q_0$ ,  $Q_{\text{ex}}$ ,  $n_2$ ,  $\alpha$ ,  $\tau$ , and  $g$ , where  $Q_0 = \omega_0/2\gamma_0$  and  $Q_{\text{ex}} = \omega_0/2\gamma_{\text{ex}}$  are the intrinsic and external coupling  $Q$  factors, respectively. Other parameters such as input power, resonator dimensions, and mode volume are provided in Supplement 1, Table S1. A genetic algorithm (GA) is implemented in MATLAB [Supplement 1, Fig. S6] to search the space of the six parameters within a reasonably constrained range to find the global best-fitting parameters by minimizing the mean squared error (MSE) between the experimental transmission spectra and calculated curve. The GA fitting routine proves to be very efficient and stable in searching for global optimum solutions, which generates a unique solution for each fitting. Figure 5 shows the example experimental and fitted transmission spectra of the silica microsphere during upscan and downscan at the five different coupling conditions. As seen in Fig. 5, the theoretical model can perfectly fit individual experimental spectrum (with R-squared evaluated to be almost 100%).

For each coupling condition and wavelength scan direction, we individually fit each spectrum and obtained the  $n_2$  and  $\alpha$  values. Comparing the resulting  $n_2$  to literature values ( $2.2\text{--}2.7 \times 10^{-20} \text{ m}^2/\text{W}$ ) [19,26,27], we notice that the downscan spectra yield better  $n_2$  measurement results than the upscan values. This shows that the individual upscan spectra are dominated by the slower thermal process, and thus are less suitable for evaluating  $n_2$ , especially when  $n_2$  is small for silica material. For deeply under-coupled conditions (upscan 1 and downscan 1 spectra in Fig. 5) where  $Q_{\text{ex}}/Q_0 > 10$ ,  $n_2$  measurement results show a larger difference from the reported values. This is likely due to the low intra-cavity power condition, which results in little effect from Kerr nonlinearity.

All conditions except for the deeply under-coupled downscan spectra [downscan 1 in Fig. 5(b)] yield consistent absorption coefficients ( $\alpha$  values between  $9.30 \times 10^{-4}/\text{m}$  and  $13.88 \times 10^{-4}/\text{m}$ ). Since the thermal effect is a slower process compared with the Kerr effect,  $\alpha$  can be better evaluated in spectra that have longer time durations (broadened spectra), where thermal build-up is more significant.

More importantly, we notice that the theoretical model with six free parameters fits individual spectrum perfectly, but there are obvious differences between the parameters obtained at different coupling conditions and scan directions. For example, the  $n_2$  values obtained from the five individually fitted downscan spectra in

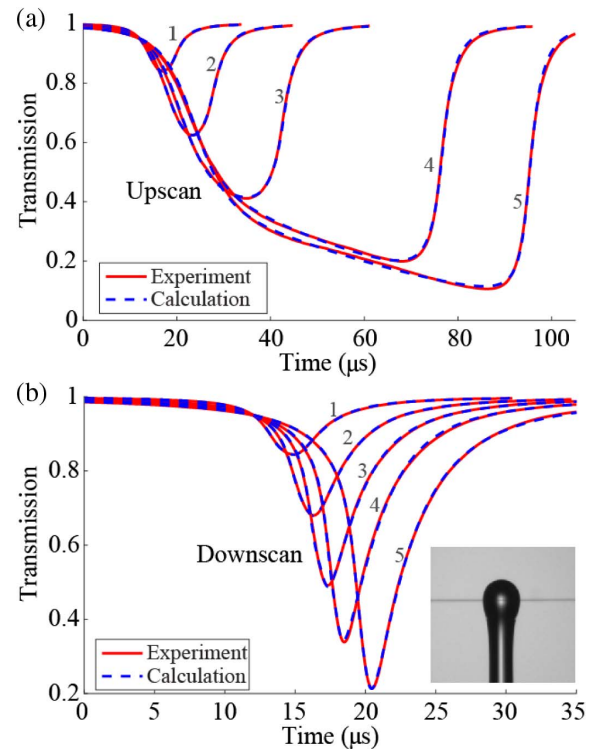


**Fig. 5.** Individually fitted experimentally measured transmission spectra of a silica microsphere resonator during (a) upscan and (b) downscan at five different coupling conditions. The inset shows the image of the silica microsphere with a radius of  $46.4 \mu\text{m}$ . The input laser power is  $6.83 \text{ mW}$ .

Fig. 5(b) range from  $1.88 \times 10^{-20}$ – $3.20 \times 10^{-20} \text{ m}^2/\text{W}$ . Therefore, it is highly likely that the model overfits individual spectra. In overfitting, the results are more sensitive to noise-induced lineshape distortion, which could explain the deviation of measured values.

To improve measurement accuracy, we include multiple spectra of different coupling conditions and scan directions in the fitting algorithm and minimize the overall fitting error on all spectra. Using the GA, we conduct fitting over four independent groups of spectra. Each group includes 2–10 spectra with different coupling conditions and scan directions (Supplement 1, Figs. S2–S5). The same number of spectra is chosen from the up and down scan directions. The average coefficient of determination, or  $R^2$  (R-squared) of the fit over each spectrum in one group is maximized. In group fitting, five common parameters ( $n_2$ ,  $\alpha$ ,  $Q_0$ ,  $\tau$ ,  $g$ ), as well as the external coupling  $Q$  factors of each spectrum are used to fit multiple spectra at the same time. All these parameters are necessary to fit the experimental data. If any of the parameters and its corresponding modality is missing, one cannot obtain a satisfactory fitting on the group of spectra. The group-fitting method yields very good fitting results over all spectra in a group with  $R^2$  values greater than 99% (Fig. 6), which is proof of the effectiveness of the theoretical model. The resulting  $\alpha$  and  $n_2$  values are given in Table 1, and the differences of values among groups are smaller than 10%. The average  $n_2$  is  $1.86 \times 10^{-20} \text{ m}^2/\text{W}$ , and the calculated average attenuation is  $9.27 \times 10^{-4}/\text{m}$ , corresponding to  $4.2 \text{ dB/km}$ . The results are self-consistent and close to reported values in literature. The result

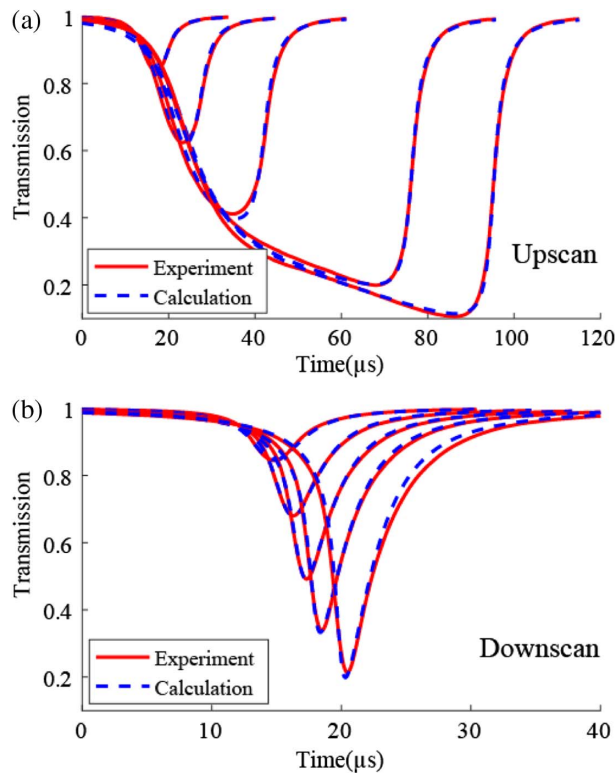


**Fig. 6.** Example of experiment (group 1 in Table 1) and group fitted transmission spectra of the silica microsphere resonator during (a) upscan and (b) downscan at five different coupling conditions. The resulting  $n_2$  value is  $1.86 \times 10^{-20} \text{ m}^2/\text{W}$ .

**Table 1. Measured  $n_2$  and  $\alpha$  Values of a Silica Microsphere for Four Independent Groups of Spectra**

Silica Microsphere	Group 1	Group 2	Group 3	Group 4
Number of spectra	10	10	4	2
$Q_0(10^7)$	1.51	1.52	1.59	1.55
$n_2(10^{-21} \text{ m}^2/\text{W})$	18.71	17.83	18.49	19.26
$\alpha(10^{-4}/\text{m})$	9.36	9.43	8.95	9.32
$\tau$ ( $\mu\text{s}$ )	143.0	141.2	168.3	191.8
$g$ (MHz)	14.4	15.1	17.9	17.5

shows that even with two spectra (one upscan and one downscan), the overfitting problem can be effectively overcome. At the same time, we also obtained important parameters of intrinsic  $Q$  factor, back-coupling rate  $g$ , and thermal time constant  $\tau$ , proving our method to be a powerful tool for microresonator characterization.

In Table 1, the parameters of  $\tau$  (143.0–191.8  $\mu\text{s}$ ) and  $g$  (14.4–17.9 MHz) show slightly larger differences among groups but are still within reasonable consistency. The dispersion of parameters among different groups can be attributed to experimental lineshape distortion induced by mechanical fluctuation of the fiber taper, taper movement due to optical gradient force from resonance light field, and laser scanning noise (Supplement 1, Fig. S7). The lineshape distortion is also responsible for the differences in the parameters obtained from individually fitted spectra. Mechanical and laser scanning noise, together with thermal effect (time constant  $> 10 \mu\text{s}$ ), has a buildup effect on the spectrum lineshape and induces lineshape distortion. Thus, the distortion due to noise is more prominent during upscan, which

has more significant thermal buildup and takes longer time than downscan. Therefore, if a single spectrum is used to measure  $n_2$ , it is better to use the down-scanned spectrum where the time of pump laser scanning across resonance is shorter. The shorter time scale of the downscan spectra means that mechanical and laser scanning noise has less accumulative effect on the spectrum, and it is better suited for evaluating Kerr nonlinearity, which is almost instantaneous (no accumulative effect). It is important to keep the input power as low as possible (to reduce significant thermal buildup) and use under-coupled conditions ( $2 < Q_{\text{ex}}/Q_0 < 10$ ), but with enough power to manifest a visible Kerr lineshape distortion. For example, downscans 2–4 in Fig. 5(b) are good candidates for individual fitting. The averaged  $n_2$  value from these spectra is  $2.3 \times 10^{-20} \text{ m}^2/\text{W}$ . This result is close to the group-fitted value of  $1.87 \times 10^{-20} \text{ m}^2/\text{W}$ , and the difference can be attributed to noise and overfitting. Other scanning methods such as thermal scanning of the microresonator, or current scanning of the pump laser, may be used to reduce the scan noise, provided the scanning mechanism is taken into consideration in the theoretical model. Once the issue of lineshape distortion is addressed, error of parameters due to overfitting on a single spectrum should be greatly reduced, and the parameters obtained from fitting of a single spectrum may be reliably used.

## B. $\text{As}_2\text{S}_3$ Microspheres

High- $Q$ -factor  $\text{As}_2\text{S}_3$  microspheres are fabricated by melting the ends of tapered  $\text{As}_2\text{S}_3$  fibers using a flame [Fig. 7(a)]. Different sizes of microspheres can be made with diameters ranging from 15  $\mu\text{m}$  to above 250  $\mu\text{m}$ . Intrinsic  $Q$  factors above  $10^6$  [Fig. 7(a)] are observed. Chalcogenide materials have much higher  $n_2$  than silica (100  $\times$  higher), and the optical absorption coefficient of these materials is orders of magnitude larger than silica. These properties allow easy observation of nonlinear lineshape distortion at lower power input in experiments. Due to the very high nonlinearity of  $\text{As}_2\text{S}_3$  material, complex phenomena such as symmetry breaking can be excited when the input power is above mW level, where the counter-propagating resonance modes are cross-phase modulated and only one directional mode is allowed [24].  $\text{As}_2\text{S}_3$  is also shown to be photosensitive in 1550 nm band [28,29]. To avoid these unwanted effects, we kept the power low ( $< 500 \mu\text{W}$ ) and used the under-coupled regime to obtain the transmission spectra.

Figures 7(b) and 7(c) show the experimental resonance spectra of the  $\text{As}_2\text{S}_3$  microsphere, showing lineshape broadening during a laser wavelength upscan. The power is kept low enough so that only Kerr and thermal nonlinear distortion is observed. In the last section, we prove that group fitting can overcome the issue of overfitting. Even a group of two spectra can yield good results. However, more spectra can be included in the fitting algorithm with minimal effort. Using the GA and group fitting of 12 spectra at different coupling conditions and scan directions, we obtained the  $Q$  factors,  $n_2$ ,  $\alpha$ ,  $\tau$ , and  $g$  [Table 2]. The  $R^2$  values of the fitting are greater than 98%. Other parameters used in calculation are in Supplement 1, Table S2. The measured  $n_2$  value is  $2.82 \times 10^{-18} \text{ m}^2/\text{W}$ , which agrees well with previous reports for non-photodarkened  $\text{As}_2\text{S}_3$  ( $n_2 \sim 2\text{--}3.8 \times 10^{-18} \text{ m}^2/\text{W}$ ) [30–32]. The measured  $\alpha$  value is 0.072/m, corresponding to absorption of 0.31 dB/m, which is slightly lower than the manufacturer specified value (0.5 dB/m for  $\text{As}_2\text{S}_3$  fiber).

In general, to obtain the resonance spectrum to measure  $n_2$ , the input laser power and scan parameters should be adjusted so

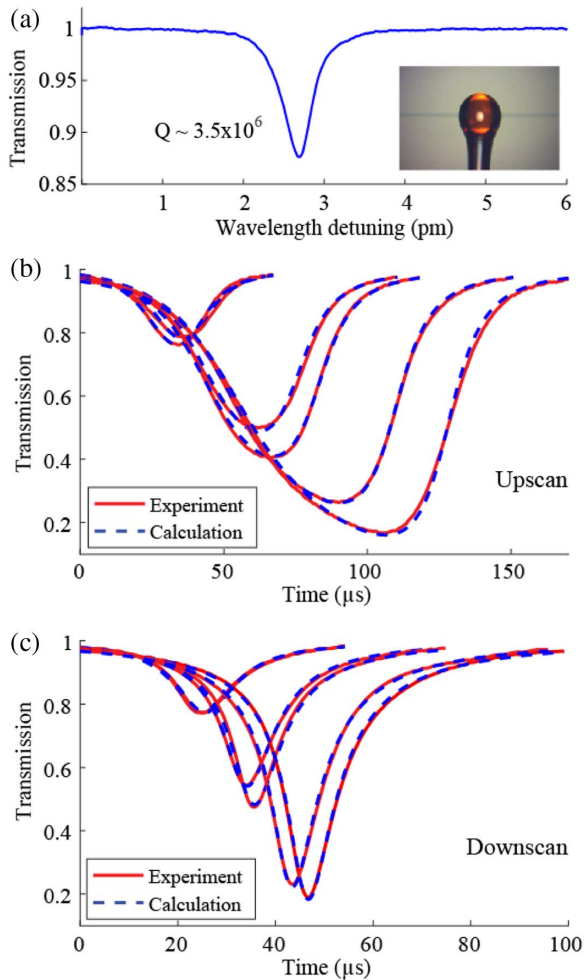


**Fig. 7.** (a) Image of the  $\text{As}_2\text{S}_3$  microsphere and its transmission spectrum at low power. The radius of the  $\text{As}_2\text{S}_3$  microsphere is  $51.5 \mu\text{m}$ , and  $Q$  factor estimated from low power, deeply under-coupled resonance linewidth is  $3.5 \times 10^6$ . (b) Experiment and group fitted transmission spectra of an  $\text{As}_2\text{S}_3$  microsphere resonator during wavelength upscan and (c) during wavelength downscan at six different coupling conditions. The input laser power is  $0.21 \text{ mW}$ , and resulting  $n_2$  value is  $2.82 \times 10^{-18} \text{ m}^2/\text{W}$ .

**Table 2. Measured  $n_2$  and  $\alpha$  Values of an  $\text{As}_2\text{S}_3$  Microsphere for a Group of 12 Spectra**

$\text{As}_2\text{S}_3$ Microsphere	Value
Number of spectra	12
$Q_0(10^7)$	0.440
$n_2(10^{-21} \text{ m}^2/\text{W})$	2821.2
$\alpha(10^{-4}/\text{m})$	720.6
$\tau (\mu\text{s})$	113.4
$g (\text{MHz})$	26.7

that only Kerr and thermal nonlinearities are manifested in the spectrum, and there is no other nonlinearity phenomenon such as symmetry breaking or Raman lasing. Under such conditions, the ringdown effect is minimal. It can be observed with high  $Q$  factors ( $>5 \times 10^7$ ) or under certain powers and scan speeds that induce significant thermal broadening (Fig. 4). Also, ringing does not affect the usefulness of our method. If thermal properties are

of particular interest, one can evaluate the thermal properties independently from the Kerr effect by using a slow scan and thermal broadening. The scanning speed should be slow enough ( $<5 \text{ nm/s}$  in  $1550 \text{ nm}$  band) that the spectrum is dominated by the thermal buildup effect [16]. Under such a condition, the Kerr broadening becomes negligible. The resulting spectrum can then be analyzed. In materials where two-photon absorption exists, such as silicon, the theoretical model can be modified to include such phenomena and still be used to quantify  $n_2$ . Two-photon absorption coefficients can also be conveniently extracted separately by using different input powers [33].

When  $g$  is larger ( $g > \gamma_0$ ), reflection modes are usually visible (Supplement 1, Section 5). If the parameter  $g$  is of particular interest, one could also record the reflected resonance mode spectrum and include it in the fitting algorithm. This could further improve the measurement accuracy of all parameters, especially  $g$ . For simplicity, we did not include reflectance in the experiments and analysis. The values of  $g$  in our experiments are smaller than the linewidth of the resonance mode; therefore, we did not observe visible mode splitting. In other words, splitting is hidden in the broader resonance linewidth.

The purpose of using multiple spectra is to avoid overfitting and error due to noise. Naturally, the fitting results are more accurate with larger numbers of experimental spectra. Our experiments show that with only two spectra (one upscan and one downscan), we are able to obtain meaningful results for five important parameters simultaneously (group 4 in Table 1).

In the case of low- $Q$  microresonators ( $Q < 10^5$ ), the simulation integration time step must be varied to account for an increased laser-cavity detuning with a general rule of timestep  $< 1/\text{detuned frequency}$ . Therefore, the calculation workload is much higher for microresonators with lower  $Q$  factors. However, a GA can be deployed using multi-threads, so a cluster can be used for faster calculation.

## 4. CONCLUSION

In summary, we developed a technique to measure the nonlinear index and absorption of microresonators from the laser-scanned transmission spectrum. The effect of  $n_2$  and  $\alpha$  on spectrum lineshape distortion is investigated through simulation and the values of  $n_2$  and  $\alpha$  of two different kinds of microresonators are evaluated in experiments. The simple experimental realization of these measurements is attractive for the study of nonlinear phenomena in microcavity structures. The theoretical model presented does not make any assumption of thermal or optical steady state and can predict complex behaviors in spectral lineshape such as broadening/narrowing, tilting, and ringing. It can be effectively used to combine with a new physical modality to accurately predict complex behavior in experiments and enable new applications. The ability to simultaneously measure the important parameters of  $n_2$ ,  $\alpha$ ,  $Q_0$ ,  $\tau$ , and  $g$  from transmission spectra is unprecedented, and can serve as the first step to characterizing a nonlinear microresonator.

Although we performed our experiments on silica and  $\text{As}_2\text{S}_3$  microspheres, our approach can be easily extended to evaluate surface modified microresonators and hybrid microresonators where two or more materials are present and can be useful in sensing applications where material property of a microresonator is changed. Furthermore, it can be applied to microresonators of different geometries (microsphere, disk, toroid, ring, and cylinder). We believe this method will greatly facilitate nonlinear optical material

studies and the application of microresonators to a variety of fields, including sensing and communications.

**Funding.** Defense Advanced Research Projects Agency (DARPA) (W911NF-15-1-0621); Air Force Office of Scientific Research (AFOSR) (FA9550-15-1-0506); University of Colorado Boulder.

**Acknowledgment.** We are grateful to Professor Tobias Kippenberg and Clément Christian Javerzac-Galy for technical assistance with chalcogenide fiber tapering.

See [Supplement 1](#) for supporting content.

## REFERENCES

- W. J. Wadsworth, A. Ortigosa-Blanch, J. C. Knight, T. A. Birks, T.-P. M. Man, and P. S. J. Russell, "Supercontinuum generation in photonic crystal fibers and optical fiber tapers: a novel light source," *J. Opt. Soc. Am. B* **19**, 2148–2155 (2002).
- F. Leo, S. Coen, P. Kockaert, S.-P. Gorza, P. Emplit, and M. Haelterman, "Temporal cavity solitons in one-dimensional Kerr media as bits in an all-optical buffer," *Nat. Photonics* **4**, 471–476 (2010).
- W. Yoshiki and T. Tanabe, "All-optical switching using Kerr effect in a silica toroid microcavity," *Opt. Express* **22**, 24332–24341 (2014).
- M. Sheik-Bahae, A. A. Said, T.-H. Wei, D. J. Hagan, and E. W. Van Stryland, "Sensitive measurement of optical nonlinearities using a single beam," *IEEE J. Quantum Electron.* **26**, 760–769 (1990).
- M. R. Krogstad, S. Ahn, W. Park, and J. T. Gopinath, "Optical characterization of chalcogenide Ge-Sb-Se waveguides at telecom wavelengths," *IEEE Photon. Technol. Lett.* **28**, 2720–2723 (2016).
- K. J. Vahala, "Optical microcavities," *Nature* **424**, 839–846 (2003).
- S. M. Spillane, T. J. Kippenberg, and K. J. Vahala, "Ultralow-threshold Raman laser using a spherical dielectric microcavity," *Nature* **415**, 621–623 (2002).
- L. Yang, D. Armani, and K. Vahala, "Fiber-coupled erbium microlasers on a chip," *Appl. Phys. Lett.* **83**, 825–826 (2003).
- F. Vollmer and L. Yang, "Review Label-free detection with high-Q microcavities: a review of biosensing mechanisms for integrated devices," *Nanophotonics (Berlin)* **1**, 267–291 (2012).
- J. G. Zhu, S. K. Ozdemir, Y. F. Xiao, L. Li, L. N. He, D. R. Chen, and L. Yang, "On-chip single nanoparticle detection and sizing by mode splitting in an ultrahigh-Q microresonator," *Nat. Photonics* **4**, 46–49 (2010).
- T. Carmon, H. Rokhsari, L. Yang, T. J. Kippenberg, and K. J. Vahala, "Temporal behavior of radiation-pressure-induced vibrations of an optical microcavity phonon mode," *Phys. Rev. Lett.* **94**, 223902 (2005).
- T. J. Kippenberg, R. Holzwarth, and S. A. Diddams, "Microresonator-based optical frequency combs," *Science* **332**, 555–559 (2011).
- B. Peng, Ş. K. Özdemir, F. Lei, F. Monifi, M. Gianfreda, G. L. Long, S. Fan, F. Nori, C. M. Bender, and L. Yang, "Parity-time-symmetric whispering-gallery microcavities," *Nat. Phys.* **10**, 394–398 (2014).
- T. Kippenberg, S. Spillane, and K. Vahala, "Kerr-nonlinearity optical parametric oscillation in an ultrahigh-Q toroid microcavity," *Phys. Rev. Lett.* **93**, 083904 (2004).
- J. Kim, M. C. Kuzyk, K. Han, H. Wang, and G. Bahl, "Non-reciprocal Brillouin scattering induced transparency," *Nat. Phys.* **11**, 275–280 (2015).
- T. Carmon, L. Yang, and K. J. Vahala, "Dynamical thermal behavior and thermal self-stability of microcavities," *Opt. Express* **12**, 4742–4750 (2004).
- Y. S. Park and H. L. Wang, "Regenerative pulsation in silica microspheres," *Opt. Lett.* **32**, 3104–3106 (2007).
- A. E. Fomin, M. L. Gorodetsky, I. S. Grudin, and V. S. Ilchenko, "Nonstationary nonlinear effects in optical microspheres," *J. Opt. Soc. Am. B* **22**, 459–465 (2005).
- A. Rasoloniaina, V. Huet, M. Thual, S. Balac, P. Féron, and Y. Dumeige, "Analysis of third-order nonlinearity effects in very high-Q WGM resonator cavity ringdown spectroscopy," *J. Opt. Soc. Am. B* **32**, 370–378 (2015).
- X. Lu, J. Y. Lee, S. Rogers, and Q. Lin, "Optical Kerr nonlinearity in a high-Q silicon carbide microresonator," *Opt. Express* **22**, 30826–30832 (2014).
- H. Rokhsari and K. J. Vahala, "Observation of Kerr nonlinearity in microcavities at room temperature," *Opt. Lett.* **30**, 427–429 (2005).
- W. Chen, J. Zhu, Ş. K. Özdemir, B. Peng, and L. Yang, "A simple method for characterizing and engineering thermal relaxation of an optical microcavity," *Appl. Phys. Lett.* **109**, 061103 (2016).
- M. Cai, O. Painter, and K. J. Vahala, "Observation of critical coupling in a fiber taper to a silica-microsphere whispering-gallery mode system," *Phys. Rev. Lett.* **85**, 74–77 (2000).
- L. Del Bino, J. M. Silver, S. L. Stebbings, and P. Del'Haye, "Symmetry breaking of counter-propagating light in a nonlinear resonator," *Sci. Rep.-Uk* **7**, 43142 (2017).
- F. Vanier, P. Bianucci, N. Godbout, M. Rochette, and Y.-A. Peter, "As 2 S 3 microspheres with near absorption-limited quality factor," in *International Conference on Optical MEMS and Nanophotonics (OMN)* (IEEE, 2012), pp. 45–46.
- K. Kim, R. Stolen, W. Reed, and K. Quoi, "Measurement of the nonlinear index of silica-core and dispersion-shifted fibers," *Opt. Lett.* **19**, 257–259 (1994).
- D. Milam, "Review and assessment of measured values of the nonlinear refractive-index coefficient of fused silica," *Appl. Opt.* **37**, 546–550 (1998).
- J. Hu, M. Torregiani, F. Morichetti, N. Carlie, A. Agarwal, K. Richardson, L. C. Kimerling, and A. Melloni, "Resonant cavity-enhanced photosensitivity in As<sub>2</sub>S<sub>3</sub> chalcogenide glass at 1550 nm telecommunication wavelength," *Opt. Lett.* **35**, 874–876 (2010).
- R. Ahmad and M. Rochette, "Photosensitivity at 1550 nm and Bragg grating inscription in As<sub>2</sub>Se<sub>3</sub> chalcogenide microwires," *Appl. Phys. Lett.* **99**, 061109 (2011).
- M. Asobe, H. Itoh, T. Miyazawa, and T. Kanamori, "Efficient and ultrafast all-optical switching using high Delta n, small core chalcogenide glass fibre," *Electron Lett.* **29**, 1966–1968 (1993).
- J. M. Laniel, N. Hô, R. Vallée, and A. Villeneuve, "Nonlinear-refractive-index measurement in As<sub>2</sub>S<sub>3</sub> channel waveguides by asymmetric self-phase modulation," *J. Opt. Soc. Am. B* **22**, 437–445 (2005).
- J. Harbold, F. Ilday, F. Wise, J. Sanghera, V. Nguyen, L. Shaw, and I. Aggarwal, "Highly nonlinear As-S-Se glasses for all-optical switching," *Opt. Lett.* **27**, 119–121 (2002).
- M. Borselli, T. J. Johnson, and O. Painter, "Accurate measurement of scattering and absorption loss in microphotonic devices," *Opt. Lett.* **32**, 2954–2956 (2007).